AMSI SUMMER RESEARCH SCHOLARSHIPS 2023–24

SET YOUR SIGHTS ON RESEARCH THIS SUMMER

Curvature dependence of wave-front speed with nonlinear diffusion

Nina Hadzivukovic
Supervised by Pascal Buenzli
Queensland University of Technology

AMSI AUSTRALIAN MATHEMATICAL SCIENCES INSTITUTE

Abstract

Tissue growth experiments on 3D-printed porous scaffolds can be modeled using reaction–diffusion Partial Differential Equations [PDEs]. We outline one such PDE that models a specific experimental application of tissue growth, and define the solution to the problem as the density of cells on a given 2-dimensional spatial domain over time. Experimental results show a distinct sharp moving wave-front, hence, assuming nonlinear diffusion is more realistic than most models, which assume diffusion to be linear resulting in smooth wave-fronts. Also observed in experiments are changes to the speed of the leading wavefront as the shape of the pore filling hole changes. The relationship between front velocity and curvature is known when diffusion is linear, we aim to extent this and derive a relationship for nonlinear diffusion. A Finite Difference [FD] method was used to find a solution to the PDE and a velocity–curvature analysis previously performed for linear diffusion was extended to include nonlinear diffusion. A generalised expression for the asymptotic prediction for the relationship between velocity and curvature was developed. When compared with local numerical estimates it was determined that like the previous linear diffusion investigation, the asymptotic prediction is only valid when the wave-front is in the travelling phase and not when the central pore is being filled.

Statement of Authorship

Contributions to this academic paper include the author Nina Hadzivukovic and supervisor Pascal Buenzli. Under the guidance and supervision of Pascal Buenzli, Nina Hadzivukovic developed MATLAB code using finite difference method to numerically determine and visualise both the linear and nonlinear solutions to the reaction-diffusion PDEs identified in [2] to accurately model tissue growth. Together they developed a generalised relationship between velocity and curvature when diffusion is nonlinear, extending velocity curvature analysis in [8] from linear to nonlinear diffusion.

Contents

1 Introduction

Reaction–diffusion waves in 2-dimensions can be used to model tissue growth in bioscaffolds and have applications in other important physical, ecological and biological systems. Experimentally it is observed that tissue growth is heavily influenced by pore geometry. Figure 1 depicts a small subset of experimental images [2] that capture the shape of the contour of the wave-front as the tissue cells proliferate and migrate over time to fill the scaffold. In these experiments, the tissues has a well defined sharp front that clearly expands into the free space as the tissue grows. The density of cells behind the wave-front increases as the wavefront moves towards the centre of the scaffold and the top view of the gridded scaffold as shown in Figure 1 indicates clear signs that the initially square wave-front approaches a circle over time.

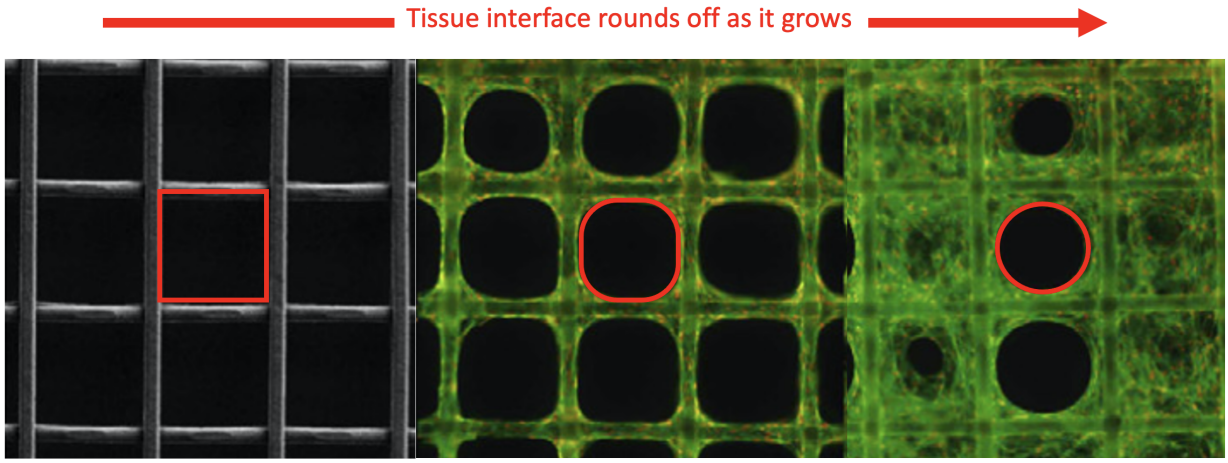

Figure 1: Images of experimental results of tissue growth on porous 3D printed scaffold. Snapshots are rescaled to capture the central 3×3 pores to highlight cell growth over time. Red line follows the shape of the contours of the wave-front of the cells which are artificially dyed green for imaging purposes. The type of cell in this experiment is the osteoblast (bone) and the green is the cytoskeleton. Adapted from [2].

In this pore bridging experiment and in general for similar tissue growing experiments, the rate at which a wave-front advances strongly depends on the curvature of the contours. Specifically in this experiment, osteoblastic cells were seeded onto the perimeter of 3D-printed scaffold square-shaped pores and grown over time to form quasi-two-dimensional sheets of tissue. The model for tissue growth is assumed to be a continuum reaction–diffusion model that describes cell density. Considering that experiments involve a very large number of cells, information about individual cells is averaged to the density. Similar models have been shown to provide very good approximations of average behaviours even for low cell numbers [2].

In a previous model using the Porous–Fisher equation

$$u_t = \nabla \cdot (D(u)\nabla u) + F(u)$$

with nonlinear diffusion, $D(u) = D_0 u$, where D_0 is a constant; tissue density u is described as a function of space and time in the out-of-plane (z) direction as a uniform layer of cells; and $F(u)$ is the reaction term. The resulting wave-front was sharp, replicating what was observed in experimental results, where movement of the leading edge of the cell population during migration maintained a well-defined sharp front. Figure 2 shows the solution to these simulations for different parameters, where the solution u is the normalised density of cells, white being 100% maximum cell capacity (given the value '1') and black is where there are no cells (given the value '0'). We define the wave-front as the time-dependent leading curve of the boundary that distinguishes where the density is nonzero, and travels in the direction of zero density. Where this boundary lies and in which it direction moves is most obvious in a cross-section taken from a constant x or y. The contours are more easily understood when looking at a top view of the solution. Each contour traces a constant density on the wave-fronts such that $u(x, y, t) = constant$.

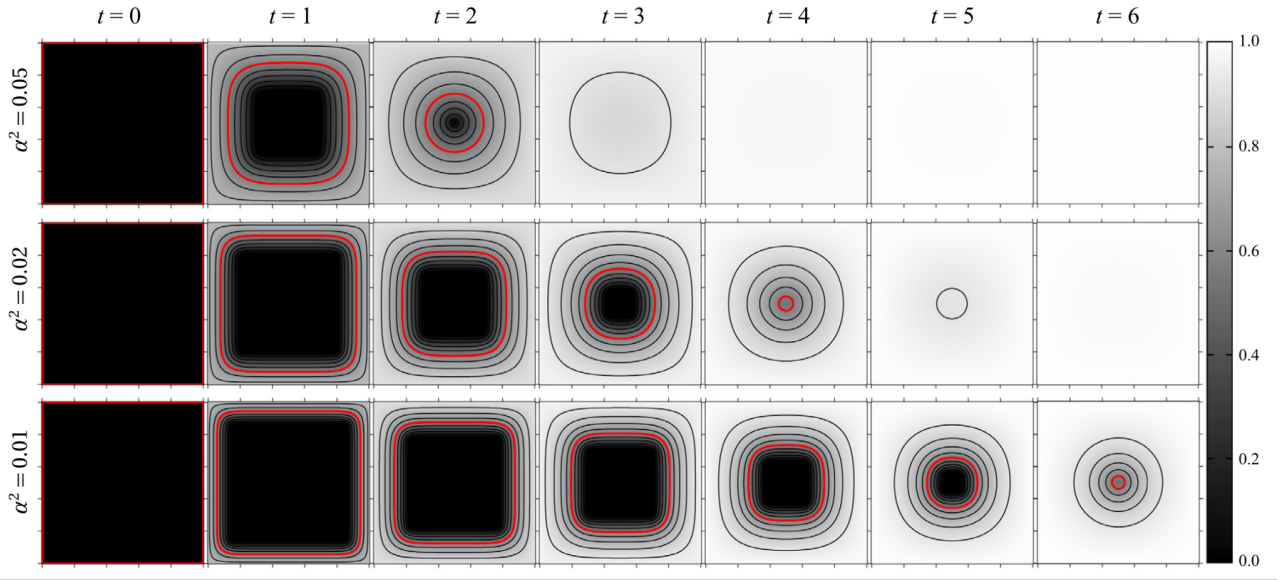

Figure 2: Frames from the nondimensionalised mathematical model at even time intervals for different combinations of the parameters taken from [2]

In the experiment the model begins with a square contour and over time as the density increases the wave-front moves towards the centre of the pore and the contour rounds off to a circle, like in Figure 1. It is difficult to determine the exact relationship between the curvature of these changing contours and the speed with which the wave-front moves towards the centre of the pore without further in depth mathematical analysis.

A velocity–curvature relationship is well defined for a similar problem with linear diffusion, where a Fisher-Kolmogorov-Petrovsky-Piskunovn (Fisher–KPP) model was used, defined by the PDE

$$u_t = D\nabla^2 u + F(u)$$

where, similar to the nonlinear KPP-Fisher model, the solution to the PDE is again $u(x, y, t)$, the density; $F(u)$ is the reaction term; and in this case, because diffusion is linear $D = D_0$, where $D = 0$ is a constant.
The asymptotic prediction for the relationship is defined as

$$v(\kappa) = c - D_0\kappa$$

where v is the velocity of the wavefront; κ is mean curvature; c is the speed of the travelling wave in the 1-dimensional problem on the infinite domain; and D_0 is the diffusivity. Though this relationship is well defined in the case of linear diffusion $D(u) = D_0$, it remains unknown how this relationship generalises to nonlinear diffusion $D(u) \neq D_0$. As experimental results show a sharp tissue-front, it is important for nonlinear diffusion be included in analysis of velocity–curvature dependence. Figure 3 highlights the difference between the solution to the problem when diffusion is linear and when diffusion is nonlinear by capturing from a cross-section of $y = 0$, the shape of the wave-fronts over time.

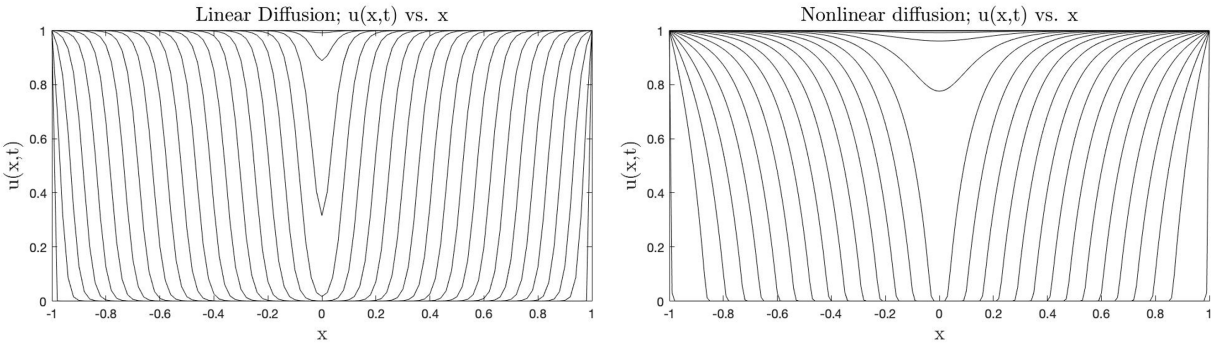

Figure 3: Comparing linear and nonlinear diffusion density solution profiles $u(x, 0, t)$ cross section of a square pore taken at $y = 0$. Profiles are shown every 1 unit of time

When we consider linear diffusion, the wave-front is smooth and does not have the sharp distinction between areas with and without cell density that we see in the case when diffusion is nonlinear. In the case of our porous scaffold experiment, it means tissue growing from opposite sided boundaries in the square will meet in the middle sooner, and the travelling wave phase of the wave-front lasts for a shorter time and for a shorter spacial distance on the same domain. Before beginning the velocity curvature analysis it is important to numerically estimate a well defined solution to the problem in question.

2 Mathematical Model

2.1 Defining the problem with nonlinear diffusion

We consider the single-species reaction diffusion model that describes the spatio-temporal evolution of u;

$$\frac{\partial}{\partial t}u = \nabla \cdot (D(u)\nabla u) + F(u)$$

where $u(\mathbf{x}, t) \geq 0$ is a density function in space $\mathbf{x}$ and time t; $D(u)$ is the diffusivity function, such that $\nabla \cdot (D(u)\nabla u)$ is the diffusion term; and $F(u)$ is the general reaction term, for example logistic growth, where $F(u) = \lambda u(1-u)$.

With linear diffusion we assume the diffusivity function to be a constant such that $D(u) = D_0$ where D_0 is a constant. When diffusion is nonlinear the diffusivity function $D(u)$ involves the density u. Depending on the application u may represent the density of chemical species, particles or cells in biological tissue, which undergo diffusive motion described by the diffusion term $\nabla \cdot (D(u)\nabla u)$ and increase according to the reaction term $F(u)$. For the investigated application of tissue growth we assume u to be the normalised density (number of cells per unit area) such that $u \in [0, 1]$, and we assume the domain to be 2-dimensional such that $\mathbf{x} = (x, y)$. We assume the density of tissue cells to be a uniform layer of the same species of cells in the z direction, and hence cell proliferation to occur in the z direction. The cell migration and hence the wavefront we are interested in occur in the $x-y$ plane with a sharp front, clearly distinguishing areas with cells and without cells. Numerical solutions $u(x, y, t)$ will be for this 2D domain.

Tissue growth experiments on porous scaffolds have previously been modeled using the Porous–Fisher equation [2], where the cell migration is modeled by the diffusion term where the diffusivity function is;

$$D(u) = D_0 u \quad : \quad D(0) = 0$$

A commonly used reaction term $F(u)$ in such applications is the logistic growth term, where;

$$F(u) = \lambda u(1-u)$$

We assume $D_0 > 0$ where D_0 is the cell diffusivity parameter and $\lambda > 0$ where λ is the proliferation rate parameter.

Both D_0 and λ depend on the tissue type in the application as they represent a cells' individual migratory and proliferative behaviour, respectively. For the application of osteoblast cells it was followed from previous literature that $D_0 = 0.005$ and $\lambda = 1$

For the tissue growth application we assume the domain to be initially empty, except for the boundary, where we set $u(x, y, 0) = 0$ in the interior of the boundary Ω. We assume inhomogeneous Dirichlet boundary conditions, where we set $u(x, y, t) = u_*$ at the boundary $\partial\Omega$, in our case $u_* = 1$, so;

$$u|_{\partial\Omega} = 1$$

2.2 Discretisation and derivation of numerical solution

Numerical solutions to the presented problem are based on an explicit Finite Difference [FD] scheme, where forward Euler method is used for time steps and central differences is applied to spatial steps.

$$u_{i,j}^{k+} = u(x_1, y_j, t_k), \quad x_i = x_{min} + i\Delta x, \quad y_j = y_{min} + j\Delta y, \quad t_k = t_{min} + k\Delta t$$

Forward Euler Method (time step numerical approximation)

$$\frac{\partial u}{\partial t} \approx \frac{u_{i,j}^{k+1} - u_{i,j}^{k}}{\Delta t}$$

Central Difference Method (spatial step numerical approximation)

$$\frac{\partial}{\partial x}\left(D(u)\frac{\partial u}{\partial x}\right) \approx \frac{1}{h}\left[\frac{D_{i+1,j}^{k} + D_{i,j}^{k}}{2}\frac{u_{i+1,j}^{k} - u_{i,j}^{k}}{h} - \frac{D_{i,j}^{k} + D_{i-1,j}^{k}}{2}\frac{u_{i,j}^{k} - u_{i-1,j}^{k}}{h}\right]$$

$$\frac{\partial}{\partial y}\left(D(u)\frac{\partial u}{\partial y}\right) \approx \frac{1}{h}\left[\frac{D_{i,j+1}^{k} + D_{i,j}^{k}}{2}\frac{u_{i,j+1}^{k} - u_{i,j}^{k}}{h} - \frac{D_{i,j}^{k} + D_{i,j-1}^{k}}{2}\frac{u_{i,j}^{k} - u_{i,j-1}^{k}}{h}\right]$$

where

$$\nabla \cdot (D(u)\nabla u) = \frac{\partial}{\partial x}\left(D(u)\frac{\partial u}{\partial x}\right) + \frac{\partial}{\partial y}\left(D(u)\frac{\partial u}{\partial y}\right)$$

The discretised problem, rearranged for $u_{i,j}^{k+1}$ (the solution to the next time-step) becomes

$$\begin{aligned} u_{i,j}^{k+1} = u_{i,j}^{k} + \frac{\Delta t}{2\Delta h^2}[&(D_{i,j}^{k} + D_{i-1,j}^{k})u_{i-1,j}^{k} + (D_{i,j}^{k} + D_{i,j-1}^{k})u_{i,j-1}^{k} \\ &- (D_{i-1,j}^{k} + D_{i,j-1}^{k} + 4D_{i,j}^{k} + D_{i+1,j}^{k} + D_{i,j+1}^{k})u_{i.j}^{k} \\ &+ (D_{i+1,j}^{k} + D_{i,j}^{k})u_{i+1,j}^{k} + (D_{i,j+1}^{k} + D_{i,j}^{k})u_{i,j+1}^{k}] + \Delta t \lambda u_{i}^{k}(1 - u_{i}^{k}) \end{aligned}$$

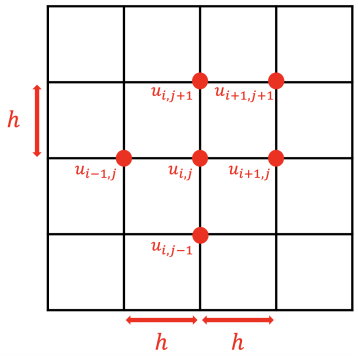

Figure 4: Visualisation of the spacial discretisation of the domain, where x is the horizontal direction and y is the vertical

Accuracy of this simple numerical solution depends on grid size and time-step size, when convergence is observed we assume the result is computationally stable. Since curvature-dependent evolution's of interfaces are known to be more sensitive to spatial discretisation [7, 1], a higher order approximation such as Runge-Kutta methods was not used for the time steps, rather the simple forward Euler method was used [8]. Spacial discretisation was in a square grid, as seen in Figure 4 where Δx and Δy are equal, so, $\Delta x = \Delta y = h$. This was chosen simplify some of the rearranging. We chose $h = 2L/N$ as it ensures our step-sizes are small enough to give an accurate numerical solution. We define $L = 1$ for our domain $[-1, 1, -1, 1]$ and $N = 200$ as the number of steps between $-L$ and L. We also use the Courant–Friedrichs–Lewy [CFL] and mad$D(u)$ convergence conditions, where for the simulations we used $\Delta t = \frac{h}{8}$.

2.3 Visualisation of the numerical solution

Starting with the known initial conditions the expression for $u_{i,j}^{k+1}$, the explicit solution for the next time-step, was iteratively calculated and the solution at different snapshots over time is visualised in Figure 5. MATLAB code was written to efficiently and accurately create the plots for cell density within the pore and cross-section over time.

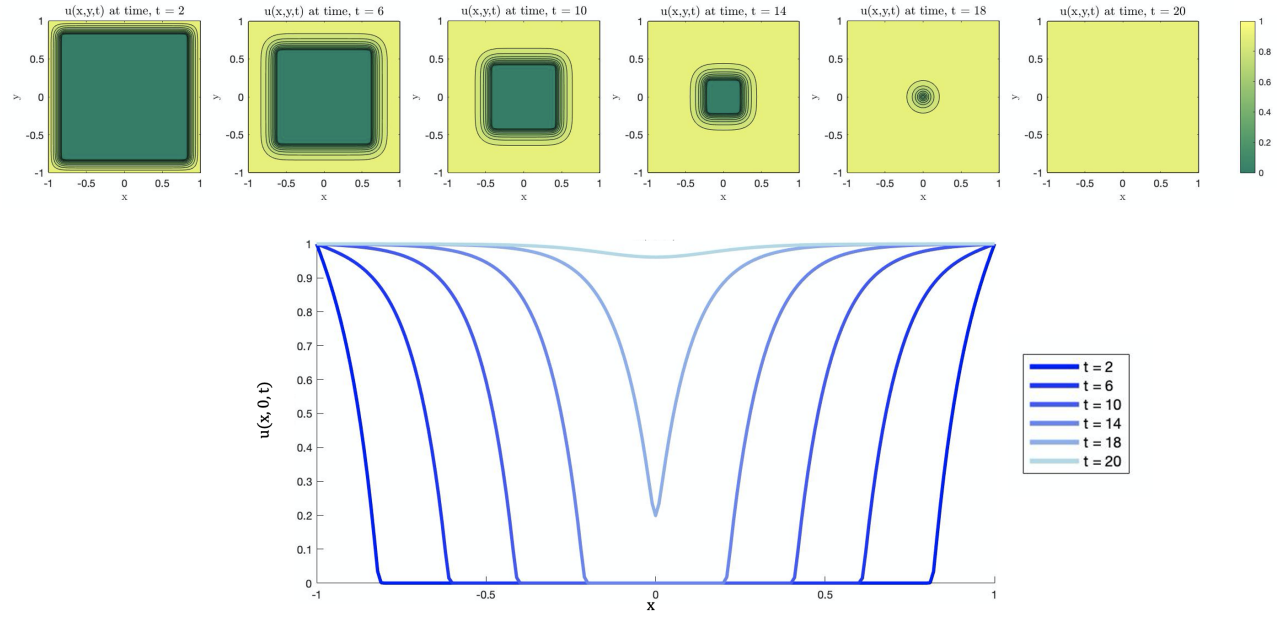

Figure 5: Snapshots of the solution $u(x, y, t)$ at increasing times, also a cross-section of the solution for the same times where $y = 0$, with $F(u) = (1u), \lambda = 1, D_0 = 0.005, h = 0.01, t = 0.001$ and Dirichlet boundary conditions $u| = 1$. Contours $u = u_c$ are shown every 0.1 increments for $u \in [0, 1]$ in black solid lines.

3 Recreating existing velocity–curvature analysis with linear diffusion

Recreating the figures from the velocity curvature analysis [8], with linear diffusion was the first step into understanding what was required to find a relationship between velocity and curvature with nonlinear diffusion. In 2-dimensions it is known that the propagation speed of the travelling wave-fronts changes according to the curvature of the contours of the wave-fronts, both experimentally and theoretically. Curvature of the contours the wavefront is a function of space and time [9, 3, 10, 2, 5]. The normal velocity v of travelling fronts is given by;

$$v = c - D\kappa$$

according to singular perturbation theories of excitable reaction–diffusion systems, where κ is the mean curvature of the wave-front and c is the speed of the travelling wave in the corresponding one-dimensional problem on

an infinite domain [9, 4, 6]. The expression is a theoretical prediction for the spatial location of the travelling wave-front as a function of time given an initial condition. In moving boundary problems such as our application of filling a pore in a square scaffold travelling wave-front velocities are used predict the time it will take to fill the given hole.

For the Fisher-KPP model with linear diffusion, outlines in previous literature, it is known that $c = 2\sqrt{D\lambda}$

The theoretical relationship between velocity and curvature is defined by;

$$v(\kappa) = w - D\kappa, \qquad where \;\; w = \frac{1}{\|\nabla u\|}\left[Du_{nn} + F(u)\right]$$

where w depends on the local solution u in the normal direction (direction of the traveling wave movement). When the wave-front is in the travelling wave phase, $v(\kappa) = w - D\kappa$ converges to $v(\kappa) = c - D\kappa$. That is, before opposing waves meet and start to fill the hole, we know that w approaches the value c, remembering that c is the wave-front speed in the 1-dimensional infinite domain problem, such that;

$$w_{1D} = \frac{1}{\|u_x\|}\left[Du_{xx} + F(u)\right] \to c$$

Given a solution u, the normal speed of the travelling wave-front is numerically estimated by [8];

$$v = \frac{u_t}{\|\nabla u\|} = \frac{1}{\|\nabla u\|}\left(D\nabla^2 u + F(u)\right) = \frac{1}{\sqrt{u_x^2 + u_y^2}}\left(Du_{xx} + Du_{yy} + F(u)\right)$$

And the mean curvature κ is numerically estimated by;

$$\kappa = \nabla \cdot \frac{\nabla u}{\|\nabla u\|} = \frac{u_{xx}u_y^2 - 2u_x u_y u_{xy} + u_{yy}u_x^2}{\left[u_x^2 + u_y^2\right]^{3/2}}$$

using second-order centred finite differences for all first-order and second-order derivatives involved.

A script in MATLAB code was created primarily to recreate previous literature plots. Recreated plots are visually equivalent to literature and validate the simulation code, such that we can be confident subsequent code created for nonlinear diffusion velocity vs. curvature will be correct, noting that modifications need to be made to incorporate nonlinear diffusion when $D(u) \neq D_0$ but $D(u) \neq D_0 u$.

When looking at the velocity vs. curvature plot, in Figure 6 it is clear that the numerical estimation better follows the trend set by the asymptotic prediction for earlier times. That is, when $t = 3$ the local estimates (blue markers) fall closer to $v(\kappa) \approx c - D\kappa$ the prediction (red line) than for $t = 7$ and $t = 15$. This is because the theoretical prediction is best when the wave is in the traveling wave phase. A cross section of the same time snapshots in Figure 6 is shown in Figure 7. It is clear that when $t = 3$ the wave is still in the traveling wave phase, however at $t = 7$ and even more so at $t = 15$ the wave-fronts have already met, and hence the wave is no longer in the traveling wave phase. For this reason the asymptotic prediction, where the local speed of the wave-front is approximated by speed of the wave-front for the 1-dimensional problem in the infinite domain, is no longer accurate, or at least not as accurate as it was for $t = 3$. This aligns with the results found in previous literature [8].

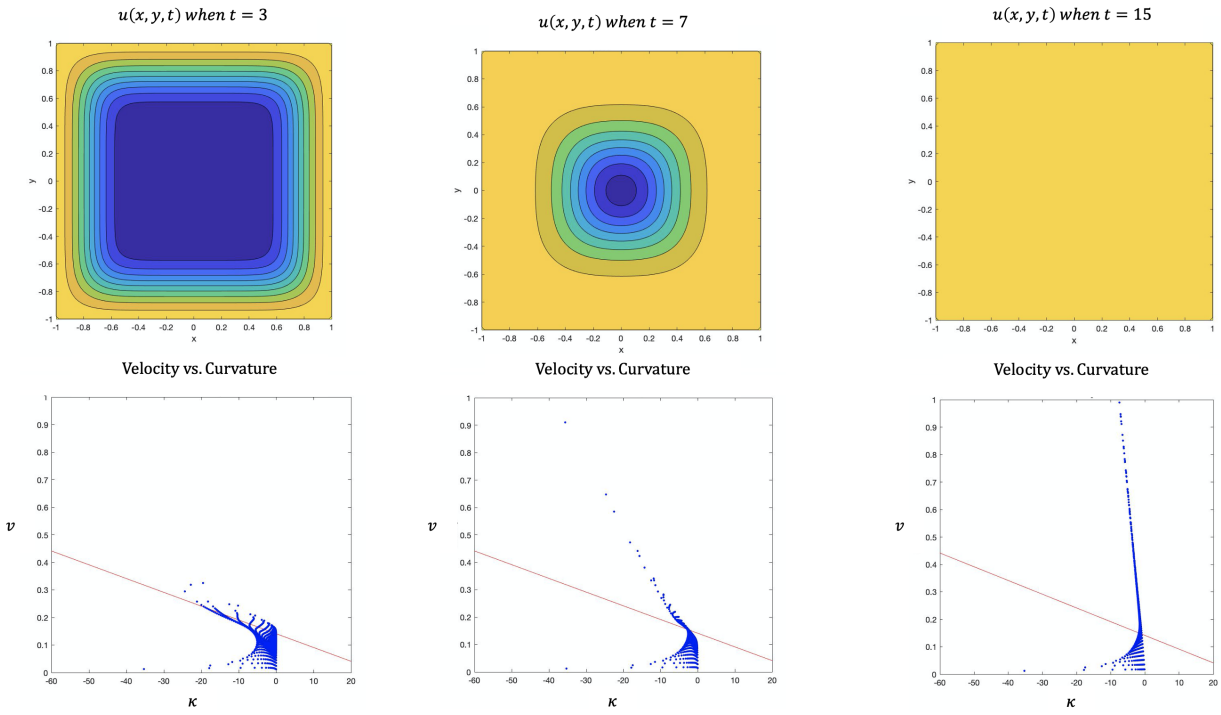

Figure 6: Snapshots of the solution $u(x, y, t)$ at different times. Recreating the curvature dependence of wave-front speed plots with linear diffusion in a square pore with $F(u) = (1u), \lambda = 1, D = 0.005, h = 0.01, t = 0.001$ and Dirichlet boundary conditions $u| = 1$. Contours $u = u_c$ are shown every 0.1 increments for $u \in [0, 1]$ in black solid lines, where yellow is where $u = 1$ and blue is where $u = 0$. The asymptotic expression $v(\kappa) \approx cD\kappa$ where $c = 2\sqrt{D\lambda}$ is shown in red in the velocity vs. curvature plots, while the local numerical estimations are shown in blue.

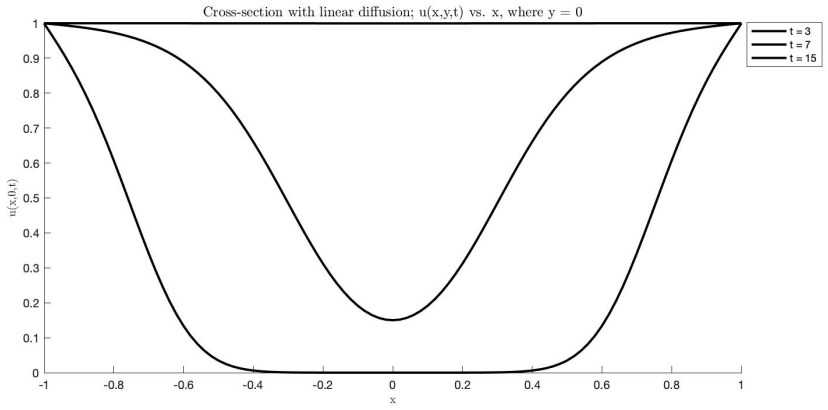

Figure 7: Cross-section of the solution $u(x, y, t)$ where $y = 0$ at the same times as Figure 6.

4 Velocity–curvature analysis with nonlinear diffusion

To determine a theoretical expression for the local relationship between the velocity and the curvature of the wavefront, we begin as in [8] by substituting the expression for the normal speed of the wavefront, into the PDE.

$$v = \frac{u_t}{\|\nabla u\|} \qquad \text{into} \qquad u_t = \nabla \cdot (D(u)\nabla u) + F(u)$$

Then, we have

$$v = \frac{1}{\|\nabla u\|} \left[\nabla \cdot (D(u)\nabla u) + F(u)\right]$$

Following similar Laplacian decomposition as described for the case with linear diffusion case [8]. The normal component of the Laplacian is $u_{nn} = \frac{\partial^2 u}{\partial n^2}$, and the transverse component of the Laplacian is $\nabla^2 u - u_{nn}$. The transverse component is proportional to the mean curvature of the travelling wavefront $\kappa = \nabla \cdot n$, so we have that

$$\nabla^2 u = u_{nn} - \kappa \|\nabla u\|$$

Finally substituting this expression for $\nabla^2 u$ into $v = \frac{1}{\|\nabla u\|}\left[\nabla D(u) \cdot \nabla u + D(u)\nabla^2 u + F(u)\right]$ we have the theoretical velocity curvature dependence

$$v(\kappa, u) = w - D(u)\kappa,$$

where

$$w(u) = \frac{1}{\|\nabla u\|}\left[\frac{\partial}{\partial n}\left(D(u)\frac{\partial}{\partial n}u\right) + F(u)\right]$$

since; $\nabla D(u) \cdot \nabla u + D(u)u_{nn} = \frac{\partial}{\partial n}\left(D(u)\frac{\partial}{\partial n}u\right)$.

For the traveling wave phase when $D(u) = D_0 u$ we assume the theoretical prediction for the spatial location of the travelling wave-front as a function of time given an initial condition is again given by

$$v = c - D(u)\kappa$$

in a traveling wave phase, where c is the speed of the travelling wave in the corresponding one-dimensional problem on an infinite domain, and $D(u) = D_0 u$. Here it is clear that v is a function not only of time and curvature but also of the density u, since D also depends on u. Hence, when the wave-front is in the travelling phase we can assume that

$$w \to c = \sqrt{\frac{D_0 \lambda}{2}}$$

For the numerical estimation, again given a solution u, the normal speed of the travelling wave-front is numerically estimated by

$$v = \frac{u_t}{\|\nabla u\|}, \qquad where \;\; u_t = \nabla \cdot (D(u)\nabla u) + F(u)$$

And the mean curvature κ is again numerically estimated by

$$\kappa = \nabla \cdot \frac{\nabla u}{\|\nabla u\|} = \frac{u_{xx}u_y^2 - 2u_x u_y u_{xy} + u_{yy}u_x^2}{\left[u_x^2 + u_y^2\right]^{3/2}}$$

using second-order centred finite differences for all first-order and second-order derivatives involved. The numerical estimations for the local speed and curvature were calculated using a similar MATLAB code structure as for the linear diffusion case. Code created in MATLAB visualised the results of the simulation and is summarised in Figure 8. Plot for the solution, cross-section and velocity vs. curvature where created for different time-points to show the spatial progression of the wave-front of the solution and the velocity curvature relationship over time.

4.1 Results

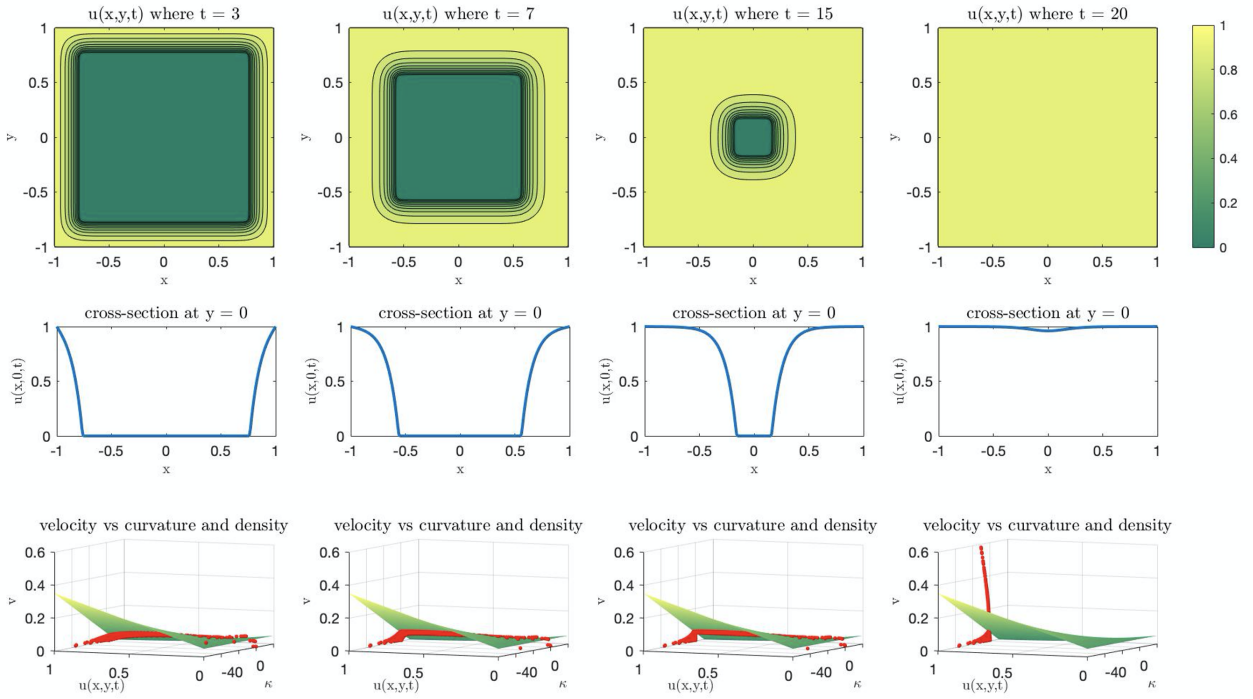

Figure 8: Results of the numerical FD method and velocity curvature analysis. Snapshots of the solution over time. A plot of the solution $u(x, y, t)$, a plot of the cross-section where $y = 0$ and a plot of the velocity. vs curvature relationship, comparing numerical local v vs. κ with asymptotic prediction for the 1D infinite domain problem, for times $t = 3, 7, 15, 20$

Similar to the previous analysis with linear diffusion, the local numerical estimates (shown as red dots on the velocity vs. curvature plot) best follow the asymptotic prediction (green surface) when the wave-front is in the travelling phase. Because diffusion is nonlinear, the wave-front is sharp and though the spatial (x, y) domain is the same ($[-1, 1], [-1, 1]$) the wave-fronts traveling from opposite sides do not meet in the middle to fill the whole till later in time. From the cross-section in Figure 8 it is obvious that even at time $t = 15$

the two opposing wave-fronts have not yet met in the middle, and so the numerical local estimates still follow the asymptotic prediction. It is only at the final snapshot at time $t = 20$ that we can see the theoretical and numerical estimates not aligning, since the wave-fronts are no longer in the travelling phase and have in fact interacted to fill the hole in the centre of the pore.

5 Conclusion and future work

A generalised expression for the velocity of the wavefront in terms of the curvature and the density solution was developed for the problem where diffusion is nonlinear. This expression provides and explicit relationship between the curvature and the velocity of a wave-front. From this study into velocity–curvature analysis with nonlinear diffusion it was found that while the wave-front is in the travelling phase the numerical simulations align with the theoretical relationship. However, once the wavefront is no longer in the traveling phase and begins to fill the central hole, at later times, the theatrical prediction no longer approximates the simulation. This can be seen at time $t = 20$ in Figure 8. This is similar to results from previous investigations of velocity–curvature dependence with linear diffusion. Given the asymptotic prediction is only valid for the travelling wave phase, a model with nonlinear diffusion will generally follow the prediction for longer than a model with linear diffusion as it has a longer travelling wave phase.

Though visualisations were only created for this specific experimental application, the velocity curvature analysis is generalised and can be easily extended to similar problem by changing the domain; diffusivity constant D_0; proliferation parameter λ; reaction function $F(u)$; diffusivity function $D(u)$; initial conditions; and boundary conditions. In the future these small modifications can extend findings outlined here to other experimental applications, perhaps to model other types of tissue growth experiments or other reaction-diffusion applications all together. Further work must also be done to extent the velocity–curvature relationship to include multiple species, where the density is not just related to one cell type. Finally, further investigations could be carried out to include 3D domains, where density is now defined as a fourth dimension and curvature of the wave-front surface is a tensor.

References

[1] Buenzli PR Alias A. A level-set method for the evolution of cells and tissue during curvature-controlled growths. *Biomed. Engng.*, 2019.

[2] Wong CS McLaughlin MP Allenby MC Woodruff MA Simpson MJ Buenzli PR, Lanaro M. Cell proliferation and migration explain pore bridging dynamics in 3d printed scaffolds of different pore size.s. *Acta Biomaterialia*, 2020.

[3] Hess B Foerster P, Müller SC. Curvature and propagation velocity of chemical waves. *Science 241*, 1988.

[4] Murray JD Grindrod P, Lewis MA. A geometrical approach to wave-type solutions of excitable reaction–diffusion systems. *Proc. R. Soc. Londl*, 1991.

[5] Crank J. The mathematics of diffusion. *Oxford Press*, 1975.

[6] Kareiva P Lewis MA. Allee dynamics and the spread of invading organisms. *Theor. Pop. Biol*, 1993.

[7] Fedkiw R Osher S. Level set methods and dynamic implicit surfaces. *New York Springer*, 2003.

[8] Buenzli PR and Simpson MJ. Cortexode: Learning cortical surface reconstruction by neural odes. *The Royal Society Publishing*, 2022.

[9] Keener JP Tyson JJ. Singular perturbation theory of traveling waves in excitable media (a review). *Physica D*, 1988.

[10] Petrovskii S Volpert V. Reaction–diffusion waves in biology. *Phys. Life Rev.*, 1909.